Interaction Note Series

Note 582

November 1, 2002

A Dynamic Stability Analysis of the PML Method[†]

S. J. Yakura, D. Dietz, and A. D. Greenwood
Air Force Research Laboratory/Directed Energy Directorate
Kirtland AFB, NM 87117

Abstract

We perform a detailed dynamic stability analysis based on the unsplit-field uniaxial PML formulation and derive a dynamic stability condition for the simple, nondispersive Maxwell/PML equations. In this paper, we introduce the delayed axial field time-response functions in place of the fictitious field-dependent source terms that others have used in the usual PML analysis. Using the delayed axial field time-response functions, we are able to cast Maxwell/PML equations for the first time into the well-known state-space form of control theory. We then proceed to use usual Laplace and Fourier transforms to investigate the characteristic equation of a system for its dynamic stability. Our finding shows that it is essential to have transverse field gradients present at all times in order to stabilize PML calculations; in fact, in the absence of transverse field gradients the PML method becomes marginally unstable with axial field variables growing linearly in time for 2-dimensional problems and cubic in time for 3-dimensional problems. The linear growth is demonstrated in the actual finite-difference time-domain calculation for the TE_{10} wave propagating inside a square waveguide that exhibits 2-dimensional behavior.

[†]This work was sponsored in part by the Air Force Office of Scientific Research and in part by Directed Energy Directorate, Air Force Research Laboratory, Kirtland AFB, NM 87117 USA

TABLE OF CONTENTS

LIST OF FIGURES

I. INTRODUCTION

Despite the successful implementation of the perfectly matched layer (PML) method to absorb outgoing electromagnetic waves at the artificial boundaries of a bounded numerical volume, the question of the dynamic stability of the PML method remains [1,2,3,4]. Abarbanel and Gottlieb [1] carried out a dynamic stability analysis of Berenger's split-field PML formulation [5], and they concluded that the split-field Maxwell/PML equations are not mathematically strongly well-posed. Hence, these equations result in unstable field variables that grow linearly in time.

In this paper we present for the first time a detailed dynamic stability analysis starting with the ***un***split-field uniaxial PML formulation [6,7], and derive a dynamic stability condition for the simple, nondispersive Maxwell/PML equations. This analysis shows that the unsplit PML method also results in an unstable condition where axial field variables grow linearly in time for 2-dimensional problems and cubic in time for 3-dimensional problems. However, for PML parameter values used in most practical applications, the growth rate is so small that no significant increase in the axial field variable is expected within a typical total simulation time of interest.

II. 2-DIMENSIONAL MAXWELL/PML EQUATIONS INSIDE A UNIAXIAL ANISTROPIC PML MEDIUM

Consider an arbitrarily polarized wave, propagating in the positive x-y direction inside an isotropic medium, that is incident on a half-space, uniaxial anisotropic PML medium. The interface between the two media is located at the $x = 0$ plane with $x \geq 0$ representing the PML half-space. Inside the PML region, the 2-dimensional Maxwell equations are expressed in the frequency (ω) domain as [6,7]

$$\underline{\nabla} \times \underline{\tilde{H}}(\omega; x, y) = j\omega \underline{\underline{\tilde{S}}}^{PML}(\omega) \bullet \varepsilon_0 \varepsilon_R \underline{\tilde{E}}(\omega; x, y) \tag{1}$$

$$\underline{\nabla} \times \underline{\tilde{E}}(\omega; x, y) = -j\omega \underline{\underline{\tilde{S}}}^{PML}(\omega) \bullet \mu_0 \mu_R \underline{\tilde{H}}(\omega; x, y) \tag{2}$$

where $\underline{\tilde{E}}(\omega;x,y)$, $\underline{\tilde{H}}(\omega;x,y)$, ε_0, ε_R, μ_0, μ_R and $\underline{\underline{\tilde{S}}}^{PML}(\omega)$ are the complex ω-dependent electric field vector, the complex ω-dependent magnetic field vector, the free-space permittivity, the relative permittivity, the free-space permeability, the relative permeability, and the complex ω-dependent uniaxial anisotropic PML

tensor, respectively. Also in the above equations, we use the notation • to denote a dot product and the symbol ~ above functions to denote ω-dependence in order to distinguish them from time-dependent functions. Elements of the complex uniaxial anisotropic PML tensor, $\underline{\underline{\tilde{S}}}^{PML}(\omega)$ are given by

$$\underline{\underline{\tilde{S}}}^{PML}(\omega) = \text{diag}\left\{\frac{1}{\tilde{S}_x(\omega)}, \tilde{S}_x(\omega), \tilde{S}_x(\omega)\right\} \tag{3}$$

where "diag" is used to represent diagonal terms of a matrix and $\tilde{S}_x(\omega)$ is an ω-dependent parameter that satisfies the full impedance matching condition at the free space/PML interface. Details of the mathematical forms and properties of $\tilde{S}_x(\omega)$, which are required for proper handling of impedance matching at the free space/PML interface, are found elsewhere [8]. The most commonly used form of $\tilde{S}_x(\omega)$ in the computational electromagnetics community is

$$\tilde{S}_x(\omega) = 1 + \frac{\sigma_x}{j\omega\varepsilon_0} \quad \text{with} \quad \frac{\sigma_x}{\varepsilon_0} = \frac{\sigma_x^*}{\mu_0} \tag{4}$$

where σ_x and σ_x^* represent the PML electric and magnetic complex conductivities, respectively, which are introduced to absorb electromagnetic waves inside the PML medium.

Since the solutions to Maxwell's equations in 2-D decompose into transverse electric (TE_x) and transverse magnetic (TM_x) waves, we consider these waves separately in the next two subsections. Note that we use the subscript x to denote the reference propagation wave vector directed in the x direction along the direction of propagation following the usual convention [9].

II.A. TRANSVERSE ELECTRIC (TE_x) WAVES

For TE_x waves, (1) through (4) reduce to the following three equations for three complex ω-dependent field variables $\tilde{H}_x(\omega; x, y)$, $\tilde{H}_y(\omega; x, y)$ and $\tilde{E}_z(\omega; x, y)$:

$$[\underline{\nabla} \times \underline{\tilde{H}}(\omega; x, y)]_z = j\omega\varepsilon_0\varepsilon_R\left(1 + \frac{\sigma_x}{j\omega\varepsilon_0}\right)\tilde{E}_z(\omega; x, y) \tag{5}$$

$$[\underline{\nabla} \times \underline{\tilde{E}}(\omega; x, y)]_x = \frac{-j\omega\mu_0\mu_R}{\left(1 + \frac{\sigma_x}{j\omega\varepsilon_0}\right)}\tilde{H}_x(\omega; x, y) \tag{6}$$

$$[\underline{\nabla} \times \underline{\tilde{E}}(\omega; x, y)]_y = -j\omega\mu_0\mu_R\left(1+\frac{\sigma_x}{j\omega\varepsilon_0}\right)\tilde{H}_y(\omega; x, y) \tag{7}$$

Directly taking the inverse Fourier transforms of the above equations with some manipulation results in the following time-dependent forms:

$$\left[\frac{1}{\varepsilon_0\varepsilon_R}\left(\frac{\partial H_y(t; x, y)}{\partial x}-\frac{\partial H_x(t; x, y)}{\partial y}\right)\right]=\frac{\partial E_z(t; x, y)}{\partial t}+\frac{\sigma_x}{\varepsilon_0}E_z(t; x, y) \tag{8}$$

$$\left[\frac{1}{\mu_0\mu_R}\frac{\partial E_z(t; x, y)}{\partial y}\right]=-\frac{\partial H_x(t; x, y)}{\partial t}+\frac{\sigma_x}{\varepsilon_0}H_x(t; x, y)-\left(\frac{\sigma_x}{\varepsilon_0}\right)^2 H_x^{Delay}(t; x, y) \tag{9}$$

$$\left[-\frac{1}{\mu_0\mu_R}\frac{\partial E_z(t; x, y)}{\partial x}\right]=-\frac{\partial H_y(t; x, y)}{\partial t}-\frac{\sigma_x}{\varepsilon_0}H_y(t; x, y) \tag{10}$$

with

$$\frac{\partial H_x^{Delay}(t; x, y)}{\partial t}+\frac{\sigma_x}{\varepsilon_0}H_x^{Delay}(t; x, y)=H_x(t; x, y) \tag{11}$$

In the above, we introduced the auxiliary variable $H_x^{Delay}(t; x, y)$ in (9) to handle the delayed time-response of the axial magnetic field $H_x(t; x, y)$. It follows naturally from the inverse Fourier transform of $\tilde{H}_x(\omega; x, y)$ upon defining $\tilde{H}_x^{Delay}(\omega; x, y)$ as follows:

$$\tilde{H}_x^{Delay}(\omega; x, y) \equiv \frac{\tilde{H}_x(\omega; x, y)}{j\omega+\frac{\sigma_x}{\varepsilon_0}} \tag{12}$$

or, expressed equivalently in the time domain, as

$$H_x^{Delay}(t; x, y)=\int_{-\infty}^{t} H_x(t'; x, y)\ \exp[-(\frac{\sigma_x}{\varepsilon_0})(t-t')]\,dt' \tag{13}$$

Note that (11) is simply the differential form of the above expression (13).

The introduction of the delayed axial magnetic field time-response function, $H_x^{Delay}(t; x, y)$, in this paper differs from the usual PML analysis that has appeared to date in the literature in which a fictitious field-dependent source term is introduced as the time integral of $[\underline{\nabla} \times \underline{E}(t; x, y)]_x$ [10,11]. Because of the introduction of the delayed axial field time-response function, this paper provides a different approach of

the PML method, which we call the delayed-axial-field-convolution technique, to distinguish our approach from other approaches that use the fictitious field-dependent source, such as the Anisotropic PML (APML) technique [7]. Advantages we gain by introducing the delayed axial field time-response function are three fold: first, the wave equations can be cast into a set of first-order differential equations that are more amenable to a dynamic stability analysis in accordance with the well-known state-space form of control theory; second, linear and nonlinear dispersive material contributions can be included without much difficulty into the PML formulation by including additional first-order differential equations for linear and nonlinear dispersive materials [12,13]; and third, we can easily implement well-known numerical techniques [14], such as the piecewise-linear approximation, to solve a set of first-order differential equations in the time domain.

Casting (8) through (11) into a more compact form results in

$$\frac{\partial \underline{W}^{TE}}{\partial t} + \underline{\underline{A}}^{TE} \bullet \underline{W}^{TE} + \underline{\underline{B}}^{TE} \bullet \frac{\partial \underline{W}^{TE}}{\partial x} + \underline{\underline{C}}^{TE} \bullet \frac{\partial \underline{W}^{TE}}{\partial y} = 0 \tag{14}$$

where $\underline{W}^{TE}(t; x, y) = [\, E_z(t; x, y),\ H_x(t; x, y),\ H_x^{Delay}(t; x, y),\ H_y(t; x, y)\,]^T$, and matrices $\underline{\underline{A}}^{TE}$, $\underline{\underline{B}}^{TE}$ and $\underline{\underline{C}}^{TE}$ are given by

$$\underline{\underline{A}}^{TE} = \begin{pmatrix} \frac{\sigma_x}{\varepsilon_0} & 0 & 0 & 0 \\ 0 & \frac{-\sigma_x}{\varepsilon_0} & \left(\frac{\sigma_x}{\varepsilon_0}\right)^2 & 0 \\ 0 & -1 & \frac{\sigma_x}{\varepsilon_0} & 0 \\ 0 & 0 & 0 & \frac{\sigma_x}{\varepsilon_0} \end{pmatrix} \qquad \underline{\underline{B}}^{TE} = \begin{pmatrix} 0 & 0 & 0 & \frac{-1}{\varepsilon_0 \varepsilon_R} \\ 0 & 0 & 0 & 0 \\ 0 & 0 & 0 & 0 \\ \frac{-1}{\mu_0 \mu_R} & 0 & 0 & 0 \end{pmatrix} \tag{15-16}$$

$$\underline{\underline{C}}^{TE} = \begin{pmatrix} 0 & \frac{1}{\varepsilon_0 \varepsilon_R} & 0 & 0 \\ \frac{1}{\mu_0 \mu_R} & 0 & 0 & 0 \\ 0 & 0 & 0 & 0 \\ 0 & 0 & 0 & 0 \end{pmatrix} \tag{17}$$

To carryout the dynamic stability analysis of (14), the Laplace transform is performed in the time domain and the Fourier transform in the spatial domain. The Laplace and Fourier transformed function $\underline{\breve{\hat{W}}}^{TE}(s; k_x, k_y)$ of $\underline{W}^{TE}(t; x, y)$ is defined by

$$\underline{W}^{TE}(t;x,y)=\frac{1}{2\pi j}\int_{s_0-j\infty}^{s_0+j\infty}\exp(st)ds\frac{1}{(2\pi)^2}\int_{-\infty}^{\infty}\int_{-\infty}^{\infty}\underline{\breve{\hat{W}}}^{TE}(s;k_x,k_y)\exp(jk_x x+jk_y y)\,dk_x dk_y \tag{18}$$

with $\mathrm{Re}(s)\geq s_0$

where s is the complex variable defined in the Laplace domain and k_x and k_y are, respectively, the complex axial and transverse wave numbers defined in the Fourier domain. Note that we use the symbols $\breve{}$ and $\hat{}$ above functions, respectively, to denote Laplace and Fourier transformed functions in order to distinguish them from time-and-space dependent functions.

Upon performing Laplace and Fourier transforms, (14) becomes

$$\underline{\underline{\breve{\hat{\Omega}}}}^{TE}(s;k_x,k_y)\bullet\underline{\breve{\hat{W}}}^{TE}(s;k_x,k_y)=\underline{\hat{W}}^{TE}(t=0;k_x,k_y) \tag{19}$$

where $\underline{\underline{\breve{\hat{\Omega}}}}^{TE}(s; k_x, k_y)$ is the characteristic matrix of the TE_x wave, given by

$$\underline{\underline{\breve{\hat{\Omega}}}}^{TE}(s;k_x,k_y)=\left(s\,\underline{\underline{I}}+\underline{\underline{A}}^{TE}+jk_x\underline{\underline{B}}^{TE}+jk_y\underline{\underline{C}}^{TE}\right)=\begin{pmatrix} s+\frac{\sigma_x}{\varepsilon_0} & \frac{jk_y}{\varepsilon_0\varepsilon_R} & 0 & \frac{-jk_x}{\varepsilon_0\varepsilon_R} \\ \frac{jk_y}{\mu_0\mu_R} & s-\frac{\sigma_x}{\varepsilon_0} & \left(\frac{\sigma_x}{\varepsilon_0}\right)^2 & 0 \\ 0 & -1 & s+\frac{\sigma_x}{\varepsilon_0} & 0 \\ \frac{-jk_x}{\mu_0\mu_R} & 0 & 0 & s+\frac{\sigma_x}{\varepsilon_0} \end{pmatrix} \tag{20}$$

The dynamic stability of the system is characterized by investigating the determinant (or, equivalently, the eigenvalues) of the characteristic matrix $\underline{\underline{\breve{\hat{\Omega}}}}^{TE}(s; k_x, k_y)$. The determinant gives the following characteristic equation, relating s to k_x and k_y modes in the form of the quartic equation:

$$s^2\left[\left(s+\frac{\sigma_x}{\varepsilon_0}\right)^2+\frac{(k_x)^2}{\varepsilon_0\varepsilon_R\mu_0\mu_R}\right]+\left(s+\frac{\sigma_x}{\varepsilon_0}\right)^2\frac{(k_y)^2}{\varepsilon_0\varepsilon_R\mu_0\mu_R}=0 \tag{21}$$

II.B. TRANSVERSE MAGNETIC (TM_x) WAVES

For TM_x waves, (1) through (4) reduce to the following three equations for three complex ω-dependent field variables $\tilde{H}_z(\omega; x, y)$, $\tilde{E}_x(\omega; x, y)$ and $\tilde{E}_y(\omega; x, y)$:

$$[\underline{\nabla} \times \underline{\tilde{E}}(\omega; x, y)]_z = -j\omega\mu_0\mu_R\left(1+\frac{\sigma_x}{j\omega\varepsilon_0}\right)\tilde{H}_z(\omega; x, y) \tag{22}$$

$$[\underline{\nabla} \times \underline{\tilde{H}}(\omega; x, y)]_x = \frac{j\omega\varepsilon_0\varepsilon_R}{\left(1+\frac{\sigma_x}{j\omega\varepsilon_0}\right)}\tilde{E}_x(\omega; x, y) \tag{23}$$

$$[\underline{\nabla} \times \underline{\tilde{H}}(\omega; x, y)]_y = j\omega\varepsilon_0\varepsilon_R\left(1+\frac{\sigma_x}{j\omega\varepsilon_0}\right)\tilde{E}_y(\omega; x, y) \tag{24}$$

Following the same steps as in the TE_x wave case yields the following equations for the TM_x wave in the Laplace and Fourier domains:

$$\underline{\underline{\check{\hat{\Omega}}}}^{TM}(s; k_x, k_y) \bullet \underline{\check{\hat{W}}}^{TM}(s; k_x, k_y) = \underline{\hat{W}}^{TM}(t=0; k_x, k_y) \tag{25}$$

where $\underline{\check{\hat{W}}}^{TM}(s; k_x, k_y) = [\check{\hat{H}}_z(s; k_x, k_y), \check{\hat{E}}_x(s; k_x, k_y), \check{\hat{E}}_x^{Delay}(s; k_x, k_y), \check{\hat{E}}_y(s; k_x, k_y)]^T$ with the delayed axial electric field $\check{\hat{E}}_x^{Delay}(s; k_x, k_y)$, defined by the Laplace and Fourier transforms of

$$E_x^{Delay}(t; x, y) = \int_{-\infty}^{t} E_x(t'; x, y)\, \exp\left[-\left(\frac{\sigma_x}{\varepsilon_0}\right)(t-t')\right] dt' \tag{26}$$

and $\underline{\underline{\check{\hat{\Omega}}}}^{TM}(s; k_x, k_y)$ is the characteristic matrix of the TM_x wave, given by

$$\underline{\underline{\check{\hat{\Omega}}}}^{TM}(s; k_x, k_y) = \begin{pmatrix} s+\frac{\sigma_x}{\varepsilon_0} & \frac{-jk_y}{\mu_0\mu_R} & 0 & \frac{jk_x}{\mu_0\mu_R} \\ \frac{-jk_y}{\varepsilon_0\varepsilon_R} & s-\frac{\sigma_x}{\varepsilon_0} & \left(\frac{\sigma_x}{\varepsilon_0}\right)^2 & 0 \\ 0 & -1 & s+\frac{\sigma_x}{\varepsilon_0} & 0 \\ \frac{jk_x}{\varepsilon_0\varepsilon_R} & 0 & 0 & s+\frac{\sigma_x}{\varepsilon_0} \end{pmatrix} \tag{27}$$

Taking the determinant of the characteristic matrix, $\underline{\underline{\check{\hat{\Omega}}}}^{TM}(s; k_x, k_y)$, gives the following characteristic equation, which is exactly the same as in the TE_x wave case:

$$s^2\left[\left(s+\frac{\sigma_x}{\varepsilon_0}\right)^2+\frac{(k_x)^2}{\varepsilon_0\varepsilon_R\mu_0\mu_R}\right]+\left(s+\frac{\sigma_x}{\varepsilon_0}\right)^2\frac{(k_y)^2}{\varepsilon_0\varepsilon_R\mu_0\mu_R}=0 \tag{28}$$

III. DYNAMIC STABILITY ANALYSIS

To study (21) [or (28)], we first normalize s, k_x and k_y by setting

$$\frac{s}{\left(\frac{\sigma_x}{\varepsilon_0}\right)}\rightarrow S, \qquad \frac{\left(\frac{(k_x)^2}{\varepsilon_0\varepsilon_R\mu_0\mu_R}\right)}{\left(\frac{\sigma_x}{\varepsilon_0}\right)^2}\rightarrow (K_x)^2 \quad \text{and} \quad \frac{\left(\frac{(k_y)^2}{\varepsilon_0\varepsilon_R\mu_0\mu_R}\right)}{\left(\frac{\sigma_x}{\varepsilon_0}\right)^2}\rightarrow (K_y)^2 \tag{29-31}$$

Now, (21) [or (28)] results in the following equation:

$$S^2[(S+1)^2+(K_x)^2]+(S+1)^2(K_y)^2=0 \tag{32}$$

Since the above characteristic equation yields S for K_x and K_y modes, the dynamic stability of a system can be characterized by investigating the values of Re{S}. The system is absolutely stable for all normal modes if and only if $\mathrm{Re}\{S\}<0$. For $\mathrm{Re}\{S\}\geq 0$ any noise present in the system eventually excites the K_x and K_y modes and drives them unstable.

From (32) it is immediately apparent that if the normalized transverse wave number K_y is zero then two of the four roots are located at $S=0$ in the complex S-plane, which results in marginally unstable behavior that grows linearly in time when transformed back into the time domain. These marginally unstable roots are associated with the axial wave, relating to the axial field variable and the delayed time-response axial field variable. The other two roots are associated with the stable, incoming and outgoing transverse waves that propagate as $\exp[-(\sigma_x/\varepsilon_0)\,t \pm jk_x x]$. Looking at the form of (32), we can see the term that contributes to stabilizing the system is the real part of K_y. Physically, this means that the transverse field gradient (in the y direction) contributes to stabilizing the axial field (in the x direction) as TE_x and TM_x waves propagate into the uniaxial PML medium.

In the special case of nondecaying waves where K_x and K_y are both real and not equal to zero (which arises from $\sigma_x=0$), Re{S} can be shown to be negative for all roots S_i using a proof based on Descartes' Rule of Signs [15] (see Appendix A), implying the system is dynamically stable for the usual purely propagating waves. Unfortunately, the actual PML system is not given by only the real part of the

normalized complex axial wave number K_x; rather, it includes the imaginary part of K_x as a result of attenuating the wave amplitude by as much as 50-100 dB within ten to twenty cells of the PML as the wave propagates into the uniaxial PML medium. To investigate the effect of the imaginary part of K_x on the dynamic stability of the PML system, (32) is solved numerically using MATHEMATICA software [16] for the four complex roots [17] of the quartic equation. Shown in Fig. 1 are stability diagrams [18] that map the stable and unstable regions of the complex S-plane into the complex K_x-plane for the selected K_y values of 0.5, 0.1 and approximately zero. In these diagrams, the boundary between stable and unstable regions is obtained by searching for values of $\mathrm{Im}\{K_x\}$, for given values of $\mathrm{Re}\{K_x\}$, that satisfy the marginally unstable condition, $\mathrm{Re}\{S\} = 0$. Comparing the stability diagrams (a) through (c) in Fig. 1, we see that as the K_y value is decreased from 0.5 to 0.1 and then from 0.1 to approximately zero the PML system becomes increasing unstable as seen by the shrinking area of the stable region in the complex K_x-plane. Fig. 1(c) shows that for $K_y \approx 0$ any small nonzero value of $\mathrm{Im}\{K_x\}$ results in an unstable condition for any value of $\mathrm{Re}\{K_x\}$. From these stability diagrams we can conclude that as the transverse field gradient decreases the system becomes increasing unstable, leading eventually to the marginally unstable condition for zero transverse field gradient (i.e., $K_y = 0$) as discussed in the beginning of this section.

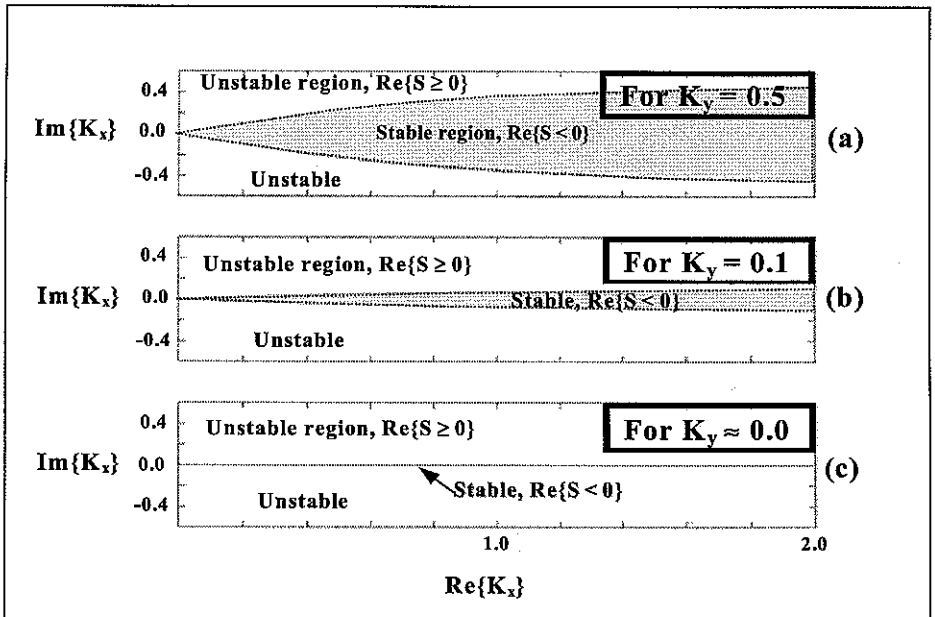

Fig. 1. Stability diagrams for mapping unstable and stable states of the complex S-plane into the complex-K_x plane for K_y values of 0.5 [top diagram (a)], 0.1 [middle diagram (b)], and approximately zero [bottom diagram (c)].

For 2-D FDTD calculations the outer most layers of the PML are bounded typically by perfect electric conductors. As a result, the transverse electric field gradient (or, equivalently, K_y) goes to zero least one spatial point within the PML for traveling modes given by even functions. It is at these spatially localized points that the PML system goes marginally unstable since there is no transverse field gradient to stabilize the marginally unstable axial field.

The spatially localized, marginally unstable behavior, which we obtain from our dynamic stability analysis, may explain the reason for some published papers reporting unstable (exponential growth) numerical PML results and others reporting stable numerical PML results, depending on the types of numerical techniques used to solve Maxwell/PML equations. Depending on which numerical technique is used, a slight numerical error from the exact solution results in deviation from a marginally unstable point, resulting in either a stable or unstable numerical condition. In second-order accurate FDTD calculations, it has been reported that an exponential time differencing technique resulted in an unstable (exponential growth) condition and a central time differencing technique resulted in a stable condition [10]. Since the PML system is found to exhibit the marginally unstable behavior specifically at the spatially localized region where the transverse field gradient is zero, we would expect the numerically calculated axial field values to grow linearly in time locally if the numerical calculation is performed correctly without numerical errors. Without going through detailed dynamic stability analysis, many researchers in the computational electromagnetics community have been lead to believe that PML systems provide stable behavior in time. As our detailed dynamic stability analysis has shown here, the simple, nondispersive PML system actually reveals the spatially localized, marginally unstable behavior and we should not expect the solution to be stable over a long time.

Now, if we are interested in getting the unconditionally stable behavior of PML systems in the long time limit, it is possible that we can achieve this goal by making slight modification in one of the Maxwell/PML equations. For TE_x waves, this can be done by reducing only the PML electric conductivity term that appears in front of H_x in (9) by a very small amount δ_x while keeping all other PML electric conductivity terms the same in (8), (9), (10) and (11) so that marginally unstable points move into the unconditionally stable region of the complex S-plane. This modification changes the characteristic matrix of the TE_x wave shown in (20) to the following form:

$$[\underline{\underline{\hat{\Omega}}}^{TE}(s;k_x,k_y)]_{\text{with }\delta_x\text{ change}} = \begin{pmatrix} s+\frac{\sigma_x}{\varepsilon_0} & \frac{jk_y}{\varepsilon_0\varepsilon_R} & 0 & \frac{-jk_x}{\varepsilon_0\varepsilon_R} \\ \frac{jk_y}{\mu_0\mu_R} & s-\frac{\sigma_x-\delta_x}{\varepsilon_0} & \left(\frac{\sigma_x}{\varepsilon_0}\right)^2 & 0 \\ 0 & -1 & s+\frac{\sigma_x}{\varepsilon_0} & 0 \\ \frac{-jk_x}{\mu_0\mu_R} & 0 & 0 & s+\frac{\sigma_x}{\varepsilon_0} \end{pmatrix} \tag{33}$$

Taking the determinant of (33) results in the following dispersion relation

$$\left[s^2+\frac{\delta_x}{\varepsilon_0}\left(s+\frac{\sigma_x}{\varepsilon_0}\right)\right]\left[\left(s+\frac{\sigma_x}{\varepsilon_0}\right)^2+\frac{(k_x)^2}{\varepsilon_0\varepsilon_R\mu_0\mu_R}\right]+\left(s+\frac{\sigma_x}{\varepsilon_0}\right)^2\frac{(k_y)^2}{\varepsilon_0\varepsilon_R\mu_0\mu_R}=0 \tag{34}$$

Evaluating (34) at $k_y = 0$ where the PML system revealed the marginally unstable behavior before, the eigenvalues of the modified PML system based on the expression in the left most bracket of (34) are given by

$$s=-\frac{\delta_x}{2\varepsilon_0}\pm\sqrt{\left(\frac{\delta_x}{2\varepsilon_0}\right)^2-\left(\frac{\delta_x}{\varepsilon_0}\right)\left(\frac{\sigma_x}{\varepsilon_0}\right)} \tag{35}$$

The above expression shows the real parts of s to be always negative for any real value $\delta_x > 0$ based on Descartes' Rule of Signs [15], implying the modified PML system for TE_x waves can be made unconditionally stable.

For TM_x waves, (27) is modified in the same way by reducing one of the PML electric conductivity terms by δ_x while keeping the others the same, which results in

$$[\underline{\underline{\hat{\Omega}}}^{TM}(s;k_x,k_y)]_{\text{with }\delta_x\text{ change}} = \begin{pmatrix} s+\frac{\sigma_x}{\varepsilon_0} & \frac{-jk_y}{\mu_0\mu_R} & 0 & \frac{jk_x}{\mu_0\mu_R} \\ \frac{-jk_y}{\varepsilon_0\varepsilon_R} & s-\frac{\sigma_x-\delta_x}{\varepsilon_0} & \left(\frac{\sigma_x}{\varepsilon_0}\right)^2 & 0 \\ 0 & -1 & s+\frac{\sigma_x}{\varepsilon_0} & 0 \\ \frac{jk_x}{\varepsilon_0\varepsilon_R} & 0 & 0 & s+\frac{\sigma_x}{\varepsilon_0} \end{pmatrix} \tag{36}$$

Taking the determinant and solving for the eigenvalues at $k_y = 0$ gives in the same unconditionally stable condition as in the TE_x wave case.

A consequence of this unconditionally stable approach is that modified PML systems no longer provide the full impedance matching condition in the presence of axial field components at the PML interface for

off-normal incident waves. However, we can choose the value of δ_x so small such that the reflection of outgoing waves back into the simulation volume of interest is within the noise level of the FDTD calculation. Hence, one advantage of this approach is that we can assure ourselves of the dynamically stable behavior of PML systems in the long time limit, provided the numerical calculation is carried out correctly.

IV. NUMERICAL VERIFICATION

To verify the dynamic stability analysis of the previous section and demonstrate the marginally unstable behavior of the axial field inside the PML in actual numerical experiments, let us consider a simple test case consisting of a rectangular X-band waveguide that is capped with a perfect electric conductor on one side and open on the other. Dimensions of the cross section of the waveguide are chosen to be 1.144 cm by 2.288 cm (in the y and z directions, respectively) to allow only a $(TE_x)_{10}$ mode to propagate in the x direction along the length of the waveguide. The length of the waveguide is chosen to be 11.44 cm. A dipole source is used to excite modes at 1.0 cm from the end that is capped.

The FDTD numerical simulation is carried out with a cubic cell size (Δx) of 0.1144 cm and a Courant number of $1/\sqrt{3}$ for the computational volume of 10x20x100 cubic cells. The dipole source provides a sinusoidal excitation of 10.0 GHz [19] that is superimposed on a Gaussian profile with the FWHM of 0.44 nanoseconds (i.e., $200\,\Delta t$). The excitation frequency is chosen to operate above the 6.557 GHz cutoff frequency of the $(TE_x)_{10}$ mode so that only the dominant $(TE_x)_{10}$ mode propagates inside the rectangular waveguide. A 10 layer PML with the fourth-order conductivity profile [$\sigma_x(x) = \sigma_x^{max}[x/(10\Delta x)]^4$] is used in front of the opening to absorb the exiting $(TE_x)_{10}$ mode. In FDTD numerical calculations, the usual Maxwell/PML equations are discretized using the usual Yee leapfrog scheme [20] based on the piecewise-linear approximation in time with exponential time differencing [21,22]. In the process of using a 3-D FDTD code and a dipole source, we let the system evolve into a $(TE_x)_{10}$ mode and made sure that only the $(TE_x)_{10}$ mode would have survived and all other modes would have decayed to the noise level within the single precision of our SUN SPARC 60 workstation after traveling a certain distance. Only after we are certain of the fact that $(TE_x)_{10}$ is the only surviving mode in the square waveguide, we place the PML a certain distance away from the dipole source to absorb the outgoing wave. Since TE_{10} is characterized by

2-D behavior, we effectively mimicked the 2-D behavior using a 3-D FDTD code. Based on the result of FDTD numerical calculations, shown in Fig. 2 is the time-dependent axial magnetic field, H_x, of the $(TE_x)_{10}$ mode that is incident on the PML layers. Fig. 3 shows a magnified view of the temporal behavior of H_x calculated at the middle of the 10^{th} PML layer for σ_x^{max} values of 2.0, 2.5 and 3.0 siemens/meter. As seen in Fig. 3, H_x grows linearly with time for all three values of σ_x^{max} as a result of having zero transverse field gradients inside the PML. To be certain of the fact that the observed linear growth is not coming from numerical discretization effects, we performed additional FDTD runs by reducing the spatial and temporal size each by a factor of 2. We see the same unstable linear growth behavior of the axial magnetic field in these runs. From curves in Fig. 3, we estimate the number of time steps required for H_x to reach 1% of the maximum axial magnetic field value to be 2.38×10^7, 7.80×10^6 and 6.22×10^6, respectively, for σ_x^{max} values of 2.0, 2.5 and 3.0 siemens/meter. These numbers are significantly larger than the total number of time steps typically chosen for many FDTD runs; hence, in most practical applications, we do not expect the field values to change significantly as a result of unstable linear growth within the total simulation time of interest.

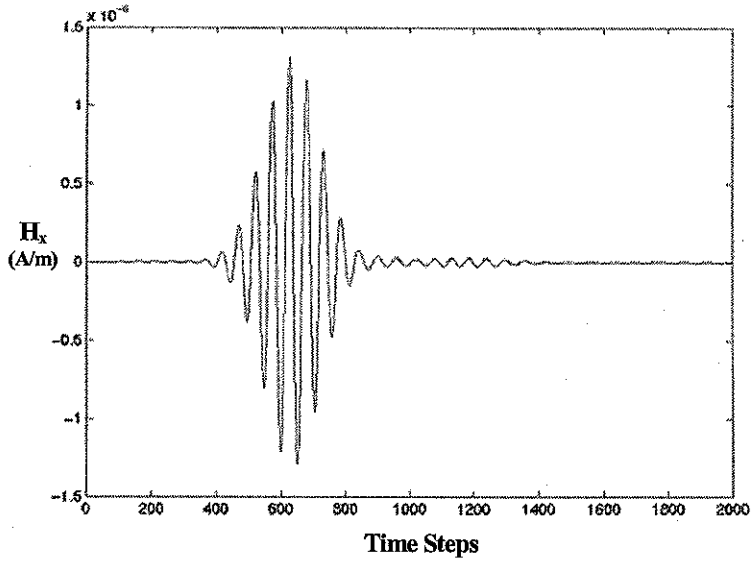

Fig. 2. Time-dependent axial electric field (H_x) incident on the PML.

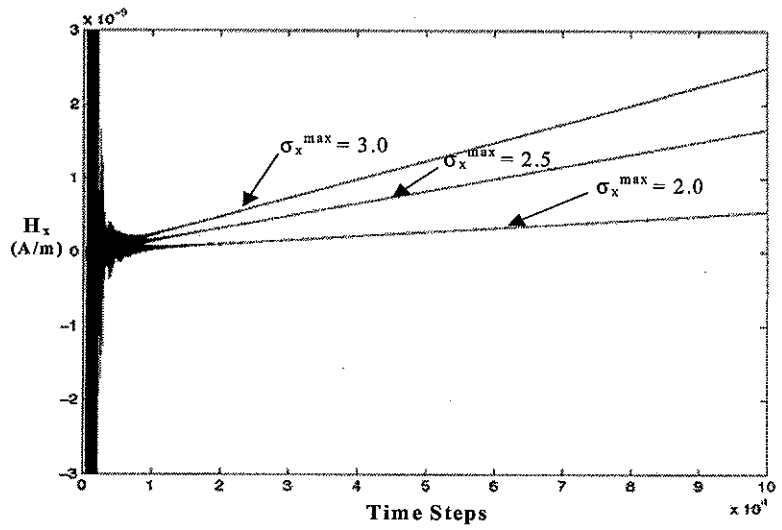

Fig. 3. A magnified view of the temporal behavior of H_x calculated along the center of a square waveguide at 10th layer of the PML for σ_x^{max} values of 2.0, 2.5 and 3.0 siemens/meter.

To check the evidence of the local marginally instability that leads to the catastrophic unstable behavior in the rest of the computational space, we performed additional FDTD calculations by simply increasing the maximum time beyond that of typical FDTD runtimes considered by people in the computational electromagnetic community (i.e., we arbitrarily set the number of maximum time steps to an order of 10^{10}). The result is that we observed the catastrophic unstable behavior that spread to the rest of the computational space. It happened after the localized axial magnetic field value grew to a point where it started impacting the calculation of transverse electric fields. At the beginning, the localized axial magnetic field grew linearly in time as predicted by our dynamic stability analysis as long as the axial magnetic field value stayed small as compared with the transverse electric field values. At later times, the transverse electric fields became unstable due to the use of Ampere's Law, which couples the marginally unstable axial magnetic field to the transverse electric fields through the gradient of the axial magnetic field. Consequently, the transverse electric fields in all surrounding cells became unstable and then spread out further to all adjacent neighboring cells as the calculation proceeded forward in time. The observed unstable behavior of transverse electric fields exhibited the exponential increase in time within the localized region of the computational space surrounding marginally unstable axial magnetic field points.

Now, if we consider the same simple test case described above and perform the FDTD calculations by solving unconditionally stable Maxwell/PML equations that we introduced in the previous section, the axial magnetic field, $H_{x,}$, shows the stable, exponentially decaying behavior in time. Shown in Fig. 4 is a magnified view of the temporal behavior of H_x that compares the results of unconditionally stable FDTD/PML calculations with that of the marginally unstable FDTD/PML case, evaluated at $\sigma_x^{max} = 2.0$ siemens/meter. The unconditionally stable FDTD/PML case clearly reveals the exponentially decaying behavior of H_x that approaches zero quickly as time goes on; on the contrary, the marginally unstable case shows the linear growth. For these unconditionally stable FDTD/PML calculations, we arbitrarily choose the δ_x value to be $1x10^{-6}$ of the σ_x value. At this δ_x value, the resulting increase in relative reflection of the modified FDTD/PML case as compared with the marginally unstable FDTD/PML case at the interface of free space and the PML turns out to be –71 dB, indicating that the impedance matching condition is met sufficiently well for the unconditionally stable PML formulation.

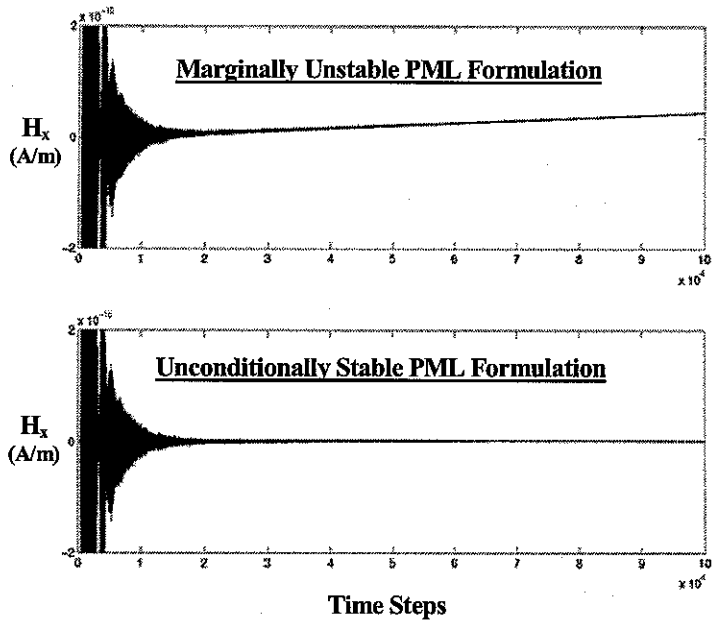

Fig. 4. A magnified view of the temporal behavior of H_x obtained along the center of a square waveguide at 5th layer of the PML for $\sigma_x^{max} = 2.0$ siemens/meter. The top diagram shows the result of the marginally unstable FDTD/PML case and the bottom diagram shows the result of the unconditionally stable FDTD/PML case.

V. EXTENSION OF THE 2-D MAXWELL/PML EQUATIONS TO 3-D FOR A UNIAXIAL ANISOTROPIC PML MEDIUM

We next extend the 2-D Maxwell/PML equations to the 3-D case. We consider an arbitrarily polarized wave, propagating in free space in the positive x-y-z direction, is incident on a half-space, uniaxial anisotropic PML medium. The interface between the two media is again located at the $x = 0$ plane with $x \geq 0$ representing the PML half-space. Inside the PML region, the 3-D Maxwell/PML equations now require the use of two complex auxiliary variables, $\breve{\hat{E}}_x^{Delay}(s; k_x, k_y, k_z)$ and $\breve{\hat{H}}_x^{Delay}(s; k_x, k_y, k_z)$, in addition to the usual six complex field variables, $\underline{\breve{\hat{H}}}(s; k_x, k_y, k_z)$ and $\underline{\breve{\hat{E}}}(s; k_x, k_y, k_z)$. Following the procedure outlined in Section II, the 3-D Maxwell/PML system can be described by the following eight-by-eight matrix system in the Laplace and Fourier domains:

$$\underline{\underline{\breve{\hat{\Omega}}}}^{EM}(s; k_x, k_y, k_z) \bullet \underline{\breve{\hat{W}}}^{EM}(s; k_x, k_y, k_z) = \underline{\hat{W}}^{EM}(t = 0; k_x, k_y, k_z) \tag{37}$$

where $\underline{\breve{\hat{W}}}^{EM}(s; k_x, k_y, k_z) = [\breve{\hat{E}}_x, \breve{\hat{E}}_x^{Delay}, \breve{\hat{E}}_y, \breve{\hat{E}}_z, \breve{\hat{H}}_x, \breve{\hat{H}}_x^{Delay}, \breve{\hat{H}}_y, \breve{\hat{H}}_z]^T$ and $\underline{\underline{\breve{\hat{\Omega}}}}^{EM}(s; k_x, k_y, k_z)$ is the characteristic matrix of the electromagnetic wave, given by

$$\underline{\underline{\breve{\hat{\Omega}}}}^{EM}(s; k_x, k_y, k_z) = \begin{pmatrix} s - \frac{\sigma_x}{\varepsilon_0} & (\frac{\sigma_x}{\varepsilon_0})^2 & 0 & 0 & 0 & 0 & \frac{jk_z}{\varepsilon_0\varepsilon_R} & \frac{-jk_y}{\varepsilon_0\varepsilon_R} \\ -1 & s + \frac{\sigma_x}{\varepsilon_0} & 0 & 0 & 0 & 0 & 0 & 0 \\ 0 & 0 & s + \frac{\sigma_x}{\varepsilon_0} & 0 & \frac{-jk_z}{\varepsilon_0\varepsilon_R} & 0 & 0 & \frac{jk_x}{\varepsilon_0\varepsilon_R} \\ 0 & 0 & 0 & s + \frac{\sigma_x}{\varepsilon_0} & \frac{jk_y}{\varepsilon_0\varepsilon_R} & 0 & \frac{-jk_x}{\varepsilon_0\varepsilon_R} & 0 \\ 0 & 0 & \frac{-jk_z}{\varepsilon_0\varepsilon_R} & \frac{jk_y}{\varepsilon_0\varepsilon_R} & s - \frac{\sigma_x}{\varepsilon_0} & (\frac{\sigma_x}{\varepsilon_0})^2 & 0 & 0 \\ 0 & 0 & 0 & 0 & -1 & s + \frac{\sigma_x}{\varepsilon_0} & 0 & 0 \\ \frac{jk_z}{\varepsilon_0\varepsilon_R} & 0 & 0 & \frac{-jk_x}{\varepsilon_0\varepsilon_R} & 0 & 0 & s + \frac{\sigma_x}{\varepsilon_0} & 0 \\ \frac{-jk_y}{\varepsilon_0\varepsilon_R} & 0 & \frac{jk_x}{\varepsilon_0\varepsilon_R} & 0 & 0 & 0 & 0 & s + \frac{\sigma_x}{\varepsilon_0} \end{pmatrix} \tag{38}$$

Taking the determinant of the characteristic matrix, $\underline{\underline{\breve{\hat{\Omega}}}}^{EM}(s; k_x, k_y, k_z)$, gives the following characteristic equation, which is simply the square of the two dimensional TE_x (or TM_x) case with $(k_y)^2$ replaced by $(k_y)^2+(k_z)^2$:

$$\left\{s^2\left[\left(s+\frac{\sigma_x}{\varepsilon_0}\right)^2+\frac{(k_x)^2}{\varepsilon_0\varepsilon_R\mu_0\mu_R}\right]+\left(s+\frac{\sigma_x}{\varepsilon_0}\right)^2\frac{(k_y)^2+(k_z)^2}{\varepsilon_0\varepsilon_R\mu_0\mu_R}\right\}^2=0 \tag{39}$$

or, expressed equivalently in normalized variables, as

$$\left\{S^2[(S+1)^2+(K_x)^2]+(S+1)^2[(K_y)^2+(K_z)^2]\right\}^2=0 \tag{40}$$

with K_z normalized the exactly the same way as in K_x and K_y.

Carrying out a dynamic stability analysis for the 3-D case similar to that in the 2-D case, we get four degenerate eigenvalues at S = 0 in the absence of the transverse gradient term (i.e., $(K_y)^2 + (K_z)^2 = 0$) that will lead to marginally unstable cubic growth in time (i.e., $\sim t^3$) when transformed back into the time domain.

In order to demonstrate marginally unstable 3-D Maxwell/PML calculations that show the actual cubic growth rate in axial fields, we believe it is rather difficult, because of the fact that a slight amount of numerical inaccuracy that comes from spatial discretization results in moving the marginally unstable points into the region of stable points in the complex S-plane. For marginally unstable cubic growth, it requires that gradients to be zero in two transverse directions all the time at a specific spatial location. In numerical (discrete) calculations, we have to make sure that a specific spatial location in question has to be resolved within the finite grid size to assure that transverse gradients to be zero all the time. It is almost analogous to placing a square tile (as of the square grid) on the top of an erupting mountain and make sure that it is balanced just right so that the tile will not slide down to the side of the mountain due to its misplacement. If the center of a tile is not placed just right at the apex of the mountain, it is most likely that the tile will fall down as a result of slight imbalance (which is equivalent to causing the gradient). In the actual numerical calculation, it is not easy to predict the exact location where two transverse gradients happen to be zero within 3-D grids, as well as placing the numerical grid right at that point such that the placement of the grid will not create an unwanted gradient. As shown in our dynamic stability analysis of the PML system, if there exist a finite transverse gradient then a system is stable. The authors predict that marginally unstable cubic growth can be seen only in the case of very fine spatial resolution calculations in which an enormous amount of computer memory is used so that the discrete space comes close to the continuum space.

VI. EXTENDING THE 2-D DYNAMIC STABILITY ANALYSIS TO CORNER REGIONS

At a corner region of the 2D PML medium, the complex uniaxial anisotropic PML tensor, $\underline{\underline{\tilde{S}}}^{PML}(\omega)$, is modified to include contributions in both x and y directions as follows:

$$\underline{\underline{\tilde{S}}}^{PML}(\omega) = \text{diag}\left\{\frac{\tilde{S}_y(\omega)}{\tilde{S}_x(\omega)}, \frac{\tilde{S}_x(\omega)}{\tilde{S}_y(\omega)}, \tilde{S}_x(\omega)\,\tilde{S}_y(\omega)\right\} \tag{41}$$

where $\tilde{S}_y(\omega)$ is given by the following form, which is identical to that of $\tilde{S}_x(\omega)$ except $\sigma_x \rightarrow \sigma_y$ and $\sigma_x^* \rightarrow \sigma_y^*$

$$\tilde{S}_y(\omega) = 1 + \frac{\sigma_y}{j\omega\varepsilon_0} \quad \text{with} \quad \frac{\sigma_y}{\varepsilon_0} = \frac{\sigma_y^*}{\mu_0} \tag{42}$$

Using (41) in (1) and (2) and following the same steps as in the previous sections yields the following equations for the TE_x wave in the Laplace and Fourier domains at the 2D PML corner region:

$$[\underline{\underline{\breve{\hat{\Omega}}}}^{TE}(s; k_x, k_y)]_{corner} \bullet [\underline{\breve{\hat{W}}}^{TE}(s; k_x, k_y)]_{corner} = [\underline{\hat{W}}^{TE}(t=0; k_x, k_y)]_{corner} \tag{43}$$

where

$$[\underline{\breve{\hat{W}}}^{TE}(s; k_x, k_y)]_{corner} = [\breve{\hat{E}}_z(s; k_x, k_y),\ \breve{\hat{H}}_x(s; k_x, k_y),\ \breve{\hat{H}}_x^{Delay}(s; k_x, k_y),\ \breve{\hat{H}}_y(s; k_x, k_y),\ \breve{\hat{H}}_y^{Delay}(s; k_x, k_y)]^T$$

and $[\underline{\underline{\breve{\hat{\Omega}}}}^{TE}(s; k_x, k_y)]_{corner}$ is the characteristic matrix of the TE_x wave, given by

$$[\underline{\underline{\breve{\hat{\Omega}}}}^{TE}(s;k_x,k_y)]_{corner} = \begin{pmatrix} s+\frac{\sigma_x+\sigma_y}{\varepsilon_0}+\frac{\sigma_x\sigma_y}{s(\varepsilon_0)^2} & \frac{jk_y}{\varepsilon_0} & 0 & \frac{-jk_x}{\varepsilon_0\varepsilon_R} & 0 \\ \frac{jk_y}{\mu_0\mu_R} & s-\frac{\sigma_x-\sigma_y}{\varepsilon_0} & \frac{\sigma_x}{\varepsilon_0}\left(\frac{\sigma_x-\sigma_y}{\varepsilon_0}\right) & 0 & 0 \\ 0 & -1 & s+\frac{\sigma_x}{\varepsilon_0} & 0 & 0 \\ \frac{-jk_x}{\mu_0\mu_R} & 0 & 0 & s-\frac{\sigma_y-\sigma_x}{\varepsilon_0} & \frac{\sigma_y}{\varepsilon_0}\left(\frac{\sigma_y-\sigma_x}{\varepsilon_0}\right) \\ 0 & 0 & 0 & -1 & s+\frac{\sigma_y}{\varepsilon_0} \end{pmatrix} \tag{44}$$

Taking the determinant of the characteristic matrix, $[\underline{\underline{\breve{\hat{\Omega}}}}^{TE}(s; k_x, k_y)]_{corner}$, gives the following characteristic equation:

$$s\left[\left(s+\frac{\sigma_x}{\varepsilon_0}\right)^2\left(s+\frac{\sigma_y}{\varepsilon_0}\right)^2+\left(s+\frac{\sigma_y}{\varepsilon_0}\right)^2\frac{(k_x)^2}{\varepsilon_0\varepsilon_R\mu_0\mu_R}+\left(s+\frac{\sigma_x}{\varepsilon_0}\right)^2\frac{(k_y)^2}{\varepsilon_0\varepsilon_R\mu_0\mu_R}\right]=0 \tag{45}$$

As seen in the above equation one root is located at $s = 0$, which gives a stable solution in the time domain, and the other four roots can be obtained by setting the expression inside the square bracket to zero. For arbitrary complex values of k_x and k_y, the real parts of the four complex roots of the quartic equation have to be investigated numerically by solving (45).

For the special case of $\sigma_x = \sigma_y$, the expression inside the square bracket of (45) reduces to the following:

$$\left(s+\frac{\sigma_x}{\varepsilon_0}\right)^2\left[\left(s+\frac{\sigma_x}{\varepsilon_0}\right)^2+\frac{(k_x)^2+(k_y)^2}{\varepsilon_0\varepsilon_R\mu_0\mu_R}\right]=0 \tag{46}$$

The first bracket of (46) results in the double root at $s = -(\sigma_x / \varepsilon_0)$, which provide the stable solutions in the time domain. The second bracket of (46) results in two more roots at $s = -(\sigma_x / \varepsilon_0) \pm j\{\sqrt{1/(\varepsilon_0\varepsilon_R\mu_0\mu_R)}\, k\}$ where $(k)^2 = (k_x)^2 + (k_y)^2$, which provide one stable and one conditionally unstable solution in the time domain. To investigate these two roots, we express k in terms of the real and imaginary parts (i.e., $k = k^R + jk^I$) so that the expression can be rewritten as

$$s=-\frac{\sigma_x}{\varepsilon_0}\pm j\left\{\sqrt{\frac{[(k^R)^2+(k^I)^2]}{\varepsilon_0\varepsilon_R\mu_0\mu_R}}\exp\left[j\tan^{-1}\left(\frac{k^I}{k^R}\right)\right]\right\},\quad (k^R\neq 0) \tag{47}$$

From (47) we can readily see that one of the two roots results in an unstable positive real value provided that the following condition is met:

$$\sqrt{\frac{[(k^R)^2+(k^I)^2]}{\varepsilon_0\varepsilon_R\mu_0\mu_R}}\sin\left[\tan^{-1}\left(\frac{k^I}{k^R}\right)\right] > \frac{\sigma_x}{\varepsilon_0} \tag{48}$$

Simplifying (48) we get

$$k^I > \sqrt{\left(\frac{\mu_0}{\varepsilon_0}\right)\varepsilon_R\mu_R}\;\sigma_x \tag{49}$$

For TM_x waves in the corner region we obtain exactly the same dynamic stability condition as shown above.

VII. CONCLUSIONS

Starting with the unsplit-field uniaxial PML formulation in the ω domain, Maxwell/PML equations are transformed into a set of first-order differential equations in time. Then, using the Laplace and Fourier transforms, the characteristic equation of the PML system is obtained and investigated for its dynamic stability.

From the dynamic stability analysis, we find that the simple, nondispersive PML system is marginally unstable due to the presence of zero transverse field gradient inside the PML where the axial field grows linearly in time for 2-dimensional problems, as demonstrated by actual numerical experiment. By making a slight modification to the usual Maxwell/PML equations, we show that the PML system can be made unconditionally stable in the long time limit, as demonstrated also by actual numerical experiment. However, there is penalty associated with obtaining the unconditionally stable behavior; that is to relax the perfectly matched impedance condition slightly.

APPENDIX A

A proof to show that the real parts of the roots of the polynomial, $S^2 [(S+1)^2 + a] + (S+1)^2 b = 0$ with positive real coefficients a and b, are all negative.

Theorem:

Consider the equation

$$S^2[(S+1)^2+a]+(S+1)^2 b=0\,,\quad S\in\mathbb{C} \tag{A.1}$$

where a, b > 0. Then

(i) (A.1) has no real solutions;

(ii) If $S_i = \alpha_i + j\beta_i$, i = 1, 2, 3, 4 ($\beta_i \neq 0$) are the roots of (A.1) then $\alpha_i < 0$, i = 1, 2, 3, 4.

Proof:

(i) Rewrite (A.1) as

$$S^2[(S+1)^2+a]=-(S+1)^2 b \tag{A.2}$$

and note that, since a, b > 0, if $S \in \mathbb{R} \setminus \{-1,0\}$ then the left hand side of (A.2) > 0 and the right hand side of (A.2) < 0, a contradiction; while if S = -1 then the left hand side of (A.2) > 0 and the right hand side of (A.2) = 0 and if S = 0 then the left hand side of (A.2) = 0 and the right hand side of (A.2) < 0, also contradictions. Thus, if S satisfies (A.1) then $S \notin \mathbb{R}$. Further, all four solutions are of the form $S = \alpha + j\beta$, $\alpha, \beta \in \mathbb{R}, \beta \neq 0$.

(ii) If $S = \alpha + j\beta$ is any solution of (A.1) then

$$(\alpha + j\beta)^2[(\alpha + j\beta + 1)^2 + a] + (\alpha + j\beta + 1)^2 b = 0 \tag{A.3}$$

Expanding and equating real and imaginary parts of (A.3) to zero gives

$$(\alpha^2 - \beta^2)^2 - 4\alpha^2\beta^2 + 2[\alpha(\alpha^2 - \beta^2) - 2\alpha\beta^2] + (1 + a + b)(\alpha^2 - \beta^2) + 2\alpha b + b = 0 \tag{A.4}$$

and

$$\beta[2\alpha(\alpha^2 - \beta^2) + 2\alpha^2 + (\alpha^2 - \beta^2) + (1 + a + b)\alpha + b] = 0 \tag{A.5}$$

In (A.5) the term in brackets must be equal to zero since, otherwise, $\beta = 0$, which is not possible since $S \notin \mathbb{R}$. Rewritten, the term results in

$$-(2\alpha + 1)\beta^2 + 2\alpha^3 + 3\alpha^2 + (1 + a + b)\alpha + b = 0 \tag{A.6}$$

If $\alpha = -½$ then we are done (since then $\alpha < 0$). Otherwise, if $\alpha \neq -½$ then (A.6) gives

$$\beta^2 = \frac{1}{2\alpha + 1}[2\alpha^3 + 3\alpha^2 + (1 + a + b)\alpha + b] \tag{A.7}$$

and

$$\beta^2 - \alpha^2 = \frac{1}{2\alpha + 1}[2\alpha^2 + (1 + a + b)\alpha + b] \tag{A.8}$$

Substituting (A.7) and (A.8) into (A.4) and simplifying leads to

$$16\alpha^6 + 48\alpha^5 + 8(7 + a + b)\alpha^4 + 16(2 + a + b)\alpha^3$$
$$+ [(1 + a + b)^2 + 8(1 + a + b)]\alpha^2 + (1 + a + b)^2\alpha + a\,b = 0 \tag{A.9}$$

Since a, b > 0 then all coefficients in (A.9) are > 0; thus, by Descartes' Rule of Signs [15], (A.9) has no positive roots. Further, zero is not a root of (A.9). Hence, all real roots of (A.9) are < 0. Finally, α_i, i = 1, 2, 3, 4 must be among the solutions of (A.9) so $\alpha_i < 0$, i = 1, 2, 3, 4.

ACKNOWLEDGEMENTS

The authors would like to acknowledge the financial help provided by Directed Energy Directorate, Air Force Research Laboratory – Phillips Site, and the partial support provided by the Air Force Office of Scientific Research for this work under Grant No. 61102F-2301-HM02.

REFERENCES

1. S. Abarbanel and D. Gottlieb, "A mathematical analysis of the PML method," Journal of Computational Physics, **134**, 357-363 (1997).
2. S. Abarbanel, D. Gottlieb, and J. S. Hesthaven, "Long time behavior of the perfectly matched layer equations in computational electromagnetics," Journal of Sci. Comput., **17**, 405-422 (2002).
3. J. W. Nehrbass, J. F. Lee and R. Lee, "Stability analysis for perfectly matched layered absorbers," Electromagnetics, **16**, 385-397 (1996).
4. F. L. Teixeira and W. C. Chew, "On causality and dynamic stability of perfectly matched layers for FDTD simulations, " IEEE Trans. Microwave Theory and Techniques, **47**, 775-785 (1999).
5. J. P. Berenger, "A perfectly matched layer for the absorption of electromagnetic waves," Journal of Computational Physics, **114**, 185-200 (1994).
6. Z. S. Sacks, D. M. Kingsland, R. Lee and J. F. Lee, "A perfectly matched anisotropic absorber for use as an absorbing boundary condition," IEEE Trans. Antennas and Propagation, **43**, 1460-1463 (1995).
7. S. D. Gedney, "An anisotropic perfectly matched layer – absorbing media for the truncation of FDTD lattices," IEEE Trans. Antennas and Propagation, **44**, 1630-1639 (1996).
8. M. Kuzuoglu and R. Mittra, "Frequency dependence of the constitutive parameters of causal perfectly matched anisotropic absorbers," IEEE Microwave and Guided Wave Letters, **6**, 447-449 (1996).
9. C. A. Balanis, *Advanced Engineering Electromagnetics*, Chapter 6: Auxiliary Vector Potential, Construction of Solutions, and Radiation And Scattering Equations (John Wiley & Sons, 1989), pp. 261-276.
10. J. C. Veihl and R. Mittra, "An efficient implementation of Berenger's perfectly matched layer (PML) for finite-difference time-domain mesh truncation," IEEE Microwave and Guided Wave Letters, **6**, 94-96 (1996).
11. L. Zhao and A. C. Cangellaris, "GT-PML: Generalized theory of perfectly matched layers and its application to the reflectionless truncation of finite-difference time-domain grids," IEEE Trans. Microwave Theory and Techniques, **44**, 2555-2563 (1996).

12. S. J. Yakura and D. Dietz, "A three-dimensional finite difference time domain – perfectly matched layer algorithm based on piecewise-linear approximation for linear dispersive media," US Air Force Technical Report AFRL-DE-TR-2000-1013, Kirtland AFB, NM, February (2000).

13. S. J. Yakura, "A three-dimensional finite difference time domain – perfectly matched layer algorithm for nonlinear dispersive media," US Air Force Technical Report AFRL-DE-TR-2000-1031, Kirtland AFB, NM, March (2000) and Dr. Carl Baum's Interaction Note Series, Note 575, Air Force Research Laboratory, April (2002); and S. J. Yakura, "A finite-difference-time-domain/perfectly-matched-layer algorithm applied for nonlinear dispersive media," *Ultra-Wideband Short-Pulse Electromagnetics 6* (Kluwer Academic/Plenum Publishers, 2003).

14. W. H. Press, S. A. Teukolsky, W. T. Vetterling and B. P. Flannery, *Numerical Recipes in FORTRAN 77 - The Art of Scientific Computing, Second Edition*, Chapter 16: Integration of ordinary differential equations (Cambridge University Press, 1992), pp. 701-744.

15. D. Cohen, *College algebra, Fourth Edition* (West Publishing Company, 1998).

16. S. Wolfram, *The MATHEMATICA Book, Fourth Edition* (Wolfram Media/Cambridge University Press, 1999).

17. W. H. Beyer, *CRC Standard Math Tables, 28th Edition* (CRC Press, Inc., 1987), pp. 12.

18. W. A. Beck and M. S. Mirotznik, "Generalized analysis of stability and numerical dispersion in the discrete-convolution FDTD method," IEEE Trans. Antennas and Propagation, **48**, 887-894 (2000).

19. D. T. Prescot and N. V. Shuley, "Reducing solution time in monochromatic FDTD waveguide simulations," IEEE Trans. Microwave Theory and Techniques, **42**, 1582-1584 (1994).

20. K. S. Yee, "Numerical solution of initial boundary value problems involving Maxwell's Equations in isotropic media," IEEE Trans. Antennas and Propagation, **AP-14**, 302-307 (1966).

21. D. F. Kelley and R. J. Luebbers, "Piecewise linear recursive convolution for dispersive media using FDTD," IEEE Trans. Antennas and Propagation, **44**, 792-797 (1996).

22. S. J. Yakura, J. T. MacGillivray and D. Dietz, "A three-dimensional finite-difference time-domain algorithm based on the recursive convolution approach for propagation of electromagnetic waves in nonlinear dispersive media," Applied Computational Electromagnetics Society (ACES) Journal, **16**, 33-44, (2001).